# Emerging and future trends in seismic attributes

*Satinder Chopra, Arcis Corporation, Calgary, Canada*
*Kurt J. Marfurt, University of Oklahoma, Norman, USA*

Seismic attributes extract information from seismic reflection data that can be used for quantitative and qualitative interpretation. Attributes are used by geologists, geophysicists, and petrophysicists to map features from basin to reservoir scale. Some attributes, such as seismic amplitude, envelope, rms amplitude, spectral magnitude, acoustic impedance, elastic impedance, and AVO are directly sensitive to changes in seismic impedance. Other attributes such as peak-to-trough thickness, peak frequency, and bandwidth are sensitive to layer thicknesses. Both classes of attributes can be quantitatively correlated to well control using multivariate analysis, geostatistics, or neural networks. Seismic attributes such as coherence, Sobel filter-based edge detectors, amplitude gradients, dip-azimuth, curvature, and gray-level co-occurrence matrix measures are directly sensitive to seismic textures and morphology. Geologic models of deposition and structural deformation coupled with seismic stratigraphy principles and seismic geomorphology allow us to qualitatively predict geologic facies.

There has been a virtual explosion in seismic attributes in the last several years. Oil and gas exploration companies, geoscience contractors, and universities continue not only to develop new seismic attributes and improve workflows using well-established attributes, but also to minimize seismic artifacts and calibrate the attribute expression of geologic features that were unrecognized or overlooked previously.

Three years ago, we were asked to provide a historical perspective on seismic attributes to celebrate the 75th anniversary of the Society of Exploration Geophysicists (Chopra and Marfurt, 2005). The goal of our contribution to this special section of *TLE* is to update readers on the progress made since that time. As in 2005, we will focus more on attributes used in mapping structure and stratigraphy, leaving attributes used in lithologic estimation and the direct detection of hydrocarbons to experts in those fields.

**Recent advances in seismic processing**. Seismic attributes enhance subtle amplitude and phase variations in the seismic signal that are often quite difficult to see on the original data. For the same reason, seismic attributes can exacerbate subtle amplitude and phase variations in seismic noise. With the exception of AVO and anisotropic velocity analysis, almost all attribute work is done on data that have already been migrated. From the seismic interpreter's point of view, there are two types of noise: those the interpreter can address through some relatively simple process applied to the migrated data volume, and those that require reprocessing of prestack data. The interpreter can address noise spikes, a limited degree of migration operator aliasing, small-velocity errors, and backscattered noise that can result in acquisition footprint, as well as overall "random noise" through band pass, $k_x$-$k_y$, and structure-oriented filtering. In contrast, significant velocity errors will result in overlapping reflector signals, producing discontinuity and tuning artifacts that may overwhelm corresponding events associated with the subsurface geology. Surface and interbed multiples result in similar strong artifacts. Our experience has been that if reflection events are highly ambiguous (such as what often occurs subsalt), attributes have only limited value. While the interpreter can play a crucial role in identifying primaries and estimating velocities through integrating well control and geologic models, fixing a prestack data set requires sending it back to a processing team.

*Suppression of acquisition footprint.* Acquisition footprint is defined as any amplitude or phase anomaly closely correlated to the surface acquisition geometry rather than to the subsurface geology. Spatially periodic changes in total fold, azimuths, and offsets give rise to spatial periodicity in enhancement of seismic signal and rejection of seismic noise. Attributes exacerbate these periodic changes, giving rise to artifacts. Gulunay (2005) and others have shown that $k_x$-$k_y$ filters can be very effective in reducing acquisition footprint on time slices for regularly sampled surveys. Since footprint due to fold, offset, and azimuth tends to be organized vertically, while that due to aliased migration artifacts is steeply dipping, $k_x$-$k_y$-$w$ or 3D running-window Radon filters may provide some additional artifact-suppression leverage. For more irregular acquisition design, the noise estimated using $k_x$-$k_y$ or $k_x$-$k_y$-$w$ filters can be followed by an adaptive filter.

For highly irregular footprint (either due to the irregularity of the survey design or to the irregularity of the near-surface conditions), filters need to be more spatially adaptive. Cvetkovic et al. (2007) and Jervis (2006) showed how wavelet transforms can suppress acquisition footprint and thus improve attribute images. Wavelet transforms are similar to running-window $k_x$-$k_y$ filters but with one major difference: they are nonlinear. The interpreter defines not only the wavelength of the noise to be suppressed, but also a threshold amplitude value. If the amplitude of a given wavelength (the so-called scale) component exceeds the threshold, that component is eliminated; otherwise it is either passed or weighted with an amplitude-dependent taper. In this manner, only the strongest (noise, with some underlying signal) events are rejected while moderate amplitude uncontaminated signal is retained.

Al-Bannagi et al. (2005) used principal component analysis to quantify the spatial pattern of acquisition footprint in the shallow part of the section. In this workflow, the interpreter needs to define the zone of interest where footprint is most clearly defined and compute a covariance matrix. Next the interpreter determines which principal components or eigenvectors (which spatial patterns) represent footprint and which might represent geologic signal. The noise patterns are then least-squares fit to and subtracted from each time slice. As with other footprint-suppression techniques, the filter is applied to the data and attributes are computed from the filtered results.

*Structure-oriented filtering*. Dip-steered mean filters work well on prestack data in which discontinuities appear as smooth diffractions, but smear faults and stratigraphic edges on migrated data. Dip-steered median and alpha-trimmed mean filters work somewhat better but will still smear faults.

Hoecker and Fehmers (2002) address this problem through an "anisotropic diffusion" smoothing algorithm. The anisotropic part is so named because the smoothing takes place parallel to the reflector, while no smoothing takes place perpendicular to the reflector. The diffusion part of the name implies that the filter is applied iteratively, much as an interpreter would apply iterative smoothing to

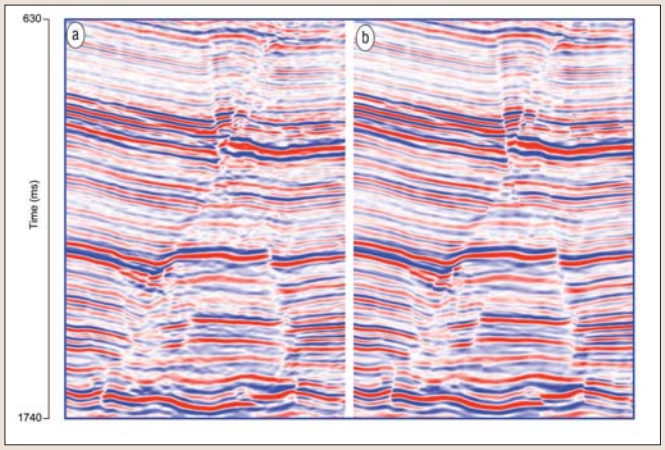


***Figure 1.*** *Segments of a seismic section—(a) before and (b) after pc filtering—from a 3D volume from Alberta, Canada. Notice the cleaner background and focused amplitudes of the seismic reflections after pc filtering as well as the preserved fault edges. (Data courtesy of Arcis Corporation.)*

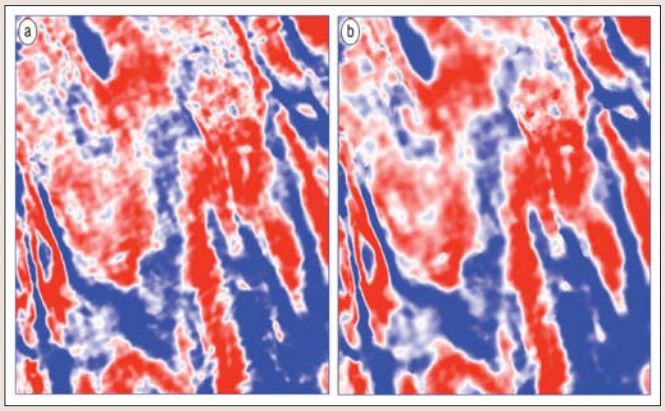


***Figure 2.*** *Time slices at 968 ms through the seismic volume generated (a) before and (b) after pc filtering of the data in Figure 1. Notice the reduced background noise and focused edges of the features after pc filtering. (Data courtesy of Arcis Corporation.)*

a time-structure map. Most important, no smoothing takes place if a discontinuity is detected, thereby preserving the appearance of major faults and stratigraphic edges. Luo et al. (2002) proposed a competing method that uses a multiwindow (Kuwahara) filter to address the same problem. Both approaches use a mean or median filter applied to data values that fall within a spatial analysis window with a thickness of one sample.

Marfurt (2006) describes a multiwindow (Kuwahara) principal component filter that uses a small volume of data samples to compute the waveform that best represents the seismic data in the spatial analysis window. Seismic processors may be more familiar with the principal component filter as equivalent to the Kohonen-Loeve (or simply KL) filter. Figure 1 shows the result of pc filtering on a seismic data set from Alberta. Notice not only the overall cleaner look of the section after pc filtering, but also the sharpening of the vertical faults. The filter was applied iteratively three times such that the end result depends on 49 neighboring traces. Figure 2 shows a similar comparison of time slices before and after pc filtering; improved event focusing and reduced background noise levels after structure-oriented filtering are clearly evident.

Figures 1 and 2 use 99 overlapping windows each of which consists of nine traces and 11 samples (± 10 ms) parallel to the dip/azimuth at the center of each window. We then apply our principal component (pc) filter to the analysis point using the window that contains the most coherent data. Because it uses (for our example 11 times) more data, the pc filter in general produces significantly better results than the corresponding mean and median filters. We advise the hopeful reader that there is no such thing as a "silver bullet" in seismic data processing. If the data are contaminated by high-amplitude spikes, then a median, alpha-trim mean, or other nonlinear filter will provide superior results. Likewise, while the pc filter will preserve amplitude variations in coherent signal, it may exacerbate acquisition footprint amplitude artifacts, whereas a mean filter will smooth them out. Structure-oriented filtering also exacerbates the fault shadow problem, which should properly be addressed through depth migration.

*Depth migration and anisotropic migration.* With the exception of complex overthrust terrains, most land seismic data volumes acquired in North America are processed through isotropic prestack time migration. The cost of prestack depth migration and of anisotropic time migration is primarily due to the iterations required to develop a more detailed velocity model. The primary impact of anisotropic migration for TI media is to increase the fold by including longer offsets that are uncontaminated by ground roll and provide greater leverage against multiples. The primary impact of prestack depth migration is to sharpen lateral terminations (both structural and stratigraphic) directly resulting in sharper attribute images. A second effect of prestack depth migration is to remove much of the velocity pull-up and push-down effects of the overburden which overprints curvature anomalies of interest in the deeper section. Finally, since attribute practitioners are often structural geologists who wish to map fractures, depth migration provides improved images of the basement which often controls shallower faulting in the shallower zone of interest (Aktepe and Marfurt, 2007).

**Spectral decomposition.** Usually seismic interpreters work with amplitude character that is based on the dominant frequency in the source wavelet. At any particular location in the subsurface, the dominant (or peak) frequency may be modified by thin layering, which further tunes the seismic reflections. Not only the amplitude but the phase of the source wavelet is affected by thin-bed tuning. Spectral decomposition provides a means of examining subsurface geologic features at any discrete frequency that falls within the acquisition bandwidth. Most commonly, these images are examined as either horizon or stratal slices where lateral changes in amplitude and phase can be directly correlated to stratigraphic features of interest.

By animating through a suite of frequencies along an interpreted horizon, a skilled interpreter can readily identify where the strata are thinning and thickening. Spectral decomposition is routinely used for thickness prediction (Partyka et al., 1999), seismic geomorphology (Marfurt and Kirlin, 2001) and direct hydrocarbon detection (Castagna et al., 2003; Sinha et al., 2005).

While the initial algorithms were based on short-window discrete Fourier and continuous wavelet transforms, Castagna et al. (2003) and Castagna and Sun (2006) developed higher-resolution algorithms, first using matching pursuit decomposition followed later by exponential decomposition techniques. Others have used the Wigner Ville distribution (Rauch-Davies and Talston, 2005; Rauch-Davies and Graham, 2006; Wankui et al., 2006) to predict fluid type, fluid distribution, reservoir quality, and reservoir delineation.

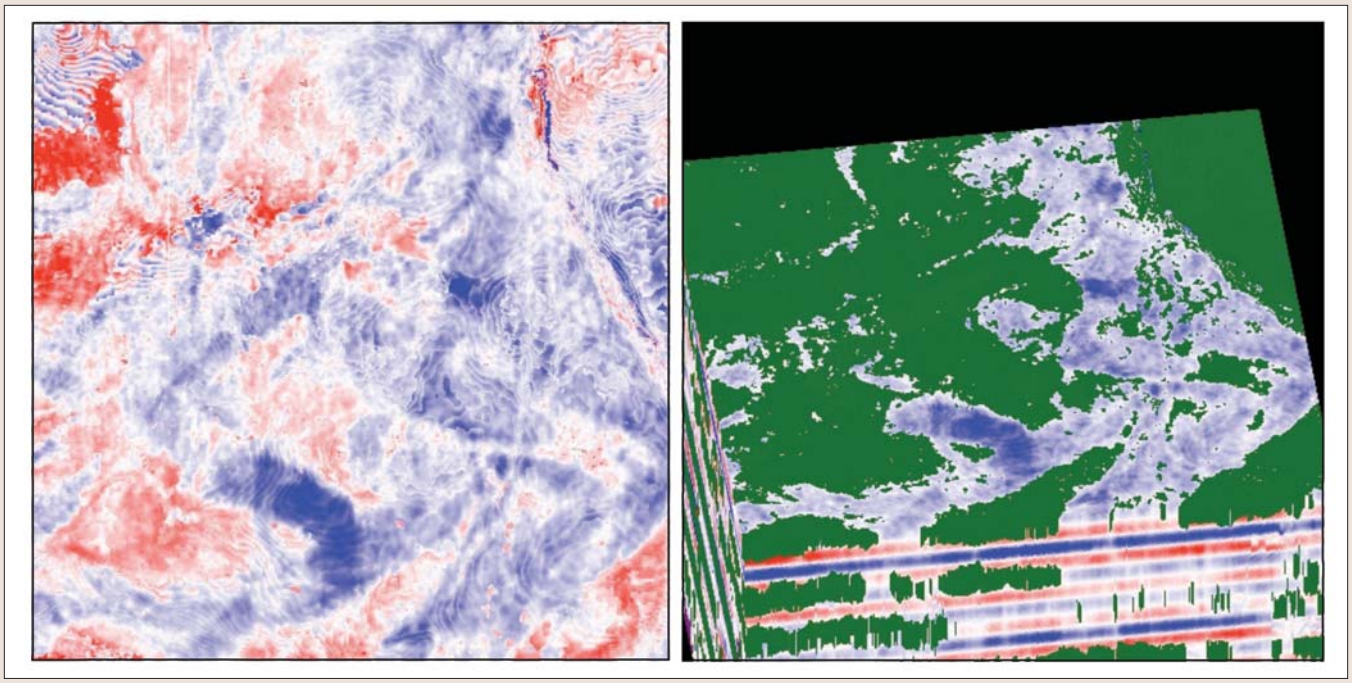

***Figure 3.*** *Comparison of a conventional stratal slice through the seismic data volume and a constant phase slice through a Wheeler volume. Green areas correspond to nondepositional hiatuses or erosional unconformities. (After Stark, 2007).*

Spectral decomposition has been applied not only to time domain, but to depth domain data as well. Montoya et al. (2005) demonstrate the application of spectral decomposition in the depth domain to an area in the Gulf of Mexico, which helped understand the distribution and classification of deepwater geologic elements.

*Discontinuities in spectra to map unconformities.* In their first paper on instantaneous attributes, Taner et al. (1979) recognized that waveform interference gives rise to discontinuities in instantaneous phase. These discontinuities in turn give rise to singularities in the time derivative of instantaneous phase, or instantaneous frequency. At first they suppressed these singularities by computing an envelope-weighted average frequency, which emphasized changes in phase near the envelope peaks where waveform interference is minimal. Later, they enhanced these discontinuities by subtracting the envelope-weighted average frequency from the instantaneous frequency, giving rise to what they called a thin-bed indicator.

*Phase unwrapping and Wheeler sections.* In the absence of waveform interference associated with unconformities and faults, the phase of a seismic trace should always monotonically increase. Stark (2006) has developed a means of unwrapping the phase in the presence of such discontinuities, thereby allowing him to generate a seismic Wheeler diagram — one that slices the data along a constant seismic phase, which is closer to a constant moment in geologic time. Imaging stratigraphic features along Wheeler surfaces using spectral components allows one to estimate the relative thickness of channel/levee complexes and also to delineate zones of nondeposition and erosion (Figure 3).

*Lipschitz-Hölder exponent measures of discontinuities.* Rather than unwrap the phase about discontinuities, Li and Liner (2008) fit spectral components with a Lipschitz-Hölder exponent, resulting in images of unconformities and condensed sections that are otherwise subtle but key to accurate seismic stratigraphic analysis. In this workflow, the interpreter uses commercial software to track unconformities that fall between seismic reflection events, rather than peaks and troughs of the events themselves. Like the Wheeler sections described above, seismic data and attributes can then be flattened along these unconformities.

*Using spectral decomposition to design band-pass filters.* Spectral decomposition allows an interpreter to quickly identify that part of the spectrum that best delineates the reservoir, allowing the construction of simple band-pass filters to optimize the seismic image for stratigraphic and/or DHI interpretation (Fahmy et al., 2005). The discovery well drilled on a West Africa field encountered 45 m of net oil pay while a sidetracked well encountered a downdip wet sand. Another well was later proposed to prove the presence of a thicker updip reservoir to evaluate its quality. However, since the seismic amplitude extraction did not support the presence of thicker or better quality sands updip from the first well, drilling was put on hold. Spectral decomposition using the matching pursuit algorithm was computed on several seismic profiles that intersected the proposed well location. Analysis of the resultant frequency gathers showed that the majority of the signal's strength for the reservoir reflections was confined to a narrow band of frequencies centered around 11 Hz and extending to just below 20 Hz. Consequently, a band-pass filter was designed and applied to the seismic data to preserve the signal bandwidth of the reservoir and attenuate all energy above 20 Hz. While the resultant data had lower resolution, a pronounced low-impedance anomaly corresponding to the reservoir was clearly visible, which significantly helped the interpretation of the stratigraphy. The well in question was later drilled and encountered 154 m of net oil sands in the target reservoir, validating the predrill prognosis of better sand facies than the first well.

*Q estimation and Q compensation.* Seismic resolution is the key to extraction of stratigraphic detail from seismic data. The broader the frequency content of the seismic data, the greater the level of seismic detail that one can extract using attributes. The effect of finite Q is not only to attenuate seismic amplitudes but also to rotate the phase. If the phase of a given frequency is rotated by more than 90° from a lower

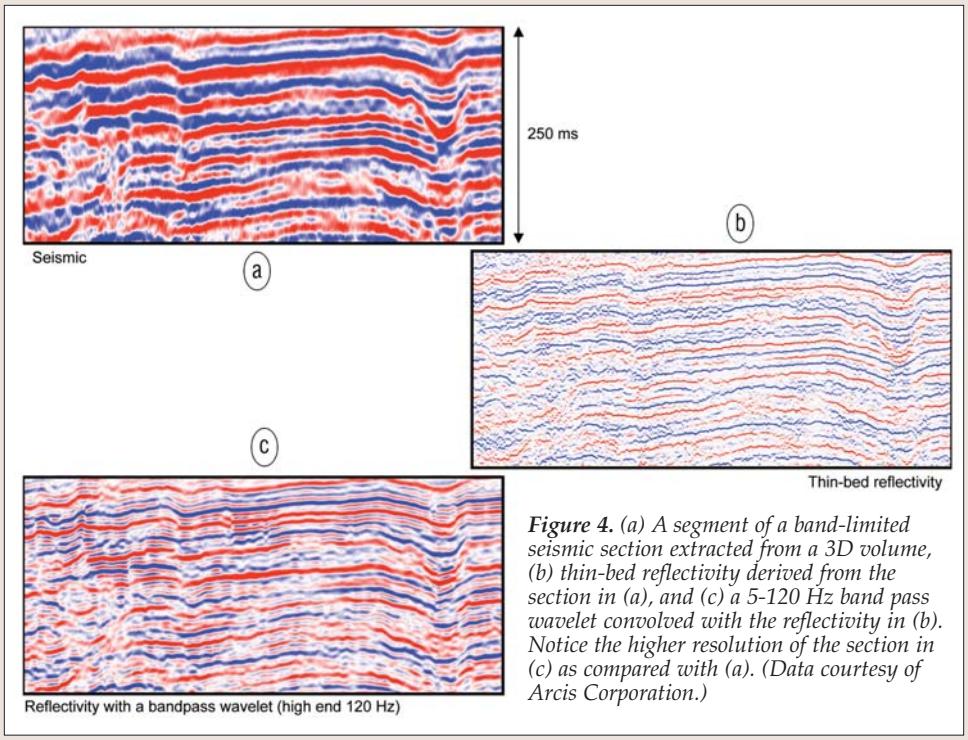


***Figure 4.*** *(a) A segment of a band-limited seismic section extracted from a 3D volume, (b) thin-bed reflectivity derived from the section in (a), and (c) a 5-120 Hz band pass wavelet convolved with the reflectivity in (b). Notice the higher resolution of the section in (c) as compared with (a). (Data courtesy of Arcis Corporation.)*

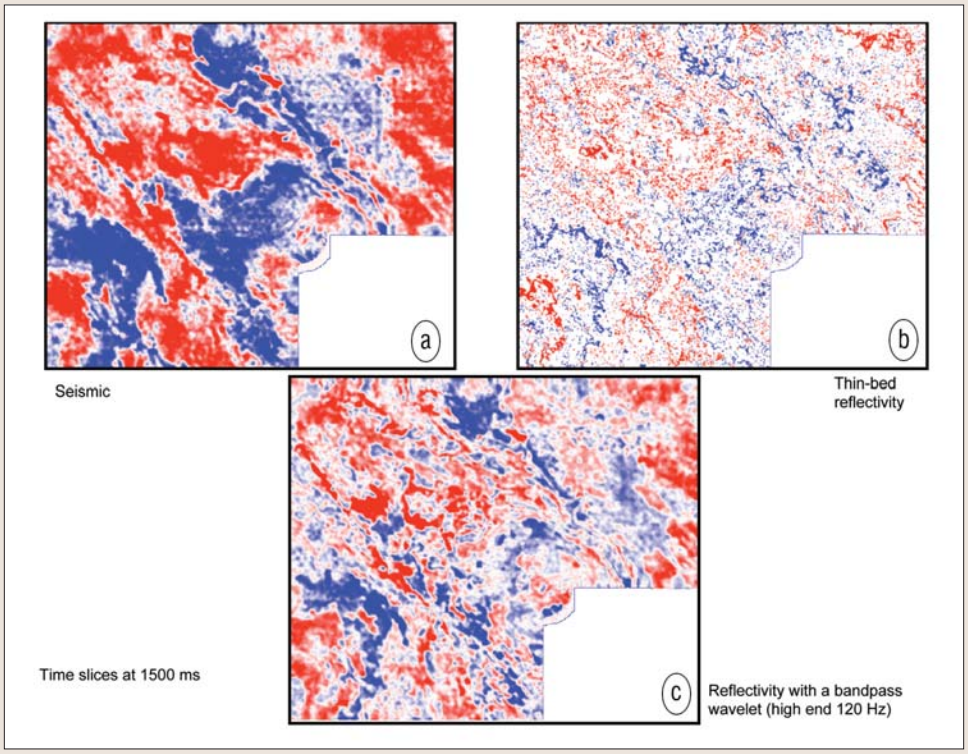


***Figure 5.*** *Time slices from (a) band-limited seismic volume, (b) thin-bed reflectivity volume derived from the seismic volume in (a), and (c) seismic volume obtained by convolving a 5–120 Hz band pass wavelet with the reflectivity in (b). The very high resolution in (b) may not yield the expected information about geology, but once a high band-pass wavelet is put on the reflectivity volume, notice the extra level of detail seen on the time slice in (c). (Data courtesy of Arcis Corporation.)*

reference frequency, no amount of amplitude compensation will allow it to constructively contribute to generating a broadband reflection. In the processing shop, poststack or prestack spectral whitening (or *Q*-compensation for seismic amplitude) is often applied to enhance the spectral bandwidth of the data prior to interpretation. Recent advances in computing spectral compon-ents have lead to improved estimation of seismic attenuation (*1/Q*) using the well-established spectral ratio technique. While *Q*-compensation is routinely applied to seismic amplitudes, *Q*-compensation applied to seismic phases is a more recent development (Wang, 2006). Based on the same model-based physics as earlier developments by Taner and Treitel (2003) and Chopra et al. (2003) that exploited the additional information provided by either well logs or VSPs, this more recent development is based on the seismic data alone.

*Spectral decomposition-based inversion for seismic reflectivity.* Thin-bed spectral inversion (Chopra et al., 2006) is a process that removes the time-variant wavelet from the seismic data and extracts the reflectivity to image thicknesses far below seismic resolution. In addition to enhanced images of thin reservoirs, these frequency-enhanced inverse images have proven very useful in mapping subtle onlaps and offlaps, thereby facilitating the mapping of parasquencies and the direction of sediment transport.

Figure 4a compares a segment of a 5–80 Hz seismic section from Alberta and its thin-bed reflectivity inversion (Figure 4b). Notice the increased detail in terms of extra cycles. Figure 4c shows the result of convolving the thin-bed reflectivity with a 5-120 Hz band-pass wavelet resulting in a high-frequency section that has more information for the interpreter. In Figure 5 we show time slices through (a) the seismic volume, (b) the thin-bed reflectivity inversion and (c) the reflectivity volume convolved with a 5-120 Hz band pass wavelet. The very fine detail on the thin-bed reflectivity time slice is too high for us to use conventional interpretation techniques. In contrast, the 5-120 Hz section shown in Figure 5c is similar to Figure 5a but shows features with much better clarity.

In Figure 6 we show stratal slices through attributes computed from both the original and higher-frequency data. Note that the improved frequency resolution does not significantly change the curvature. In contrast, the impact on coherence is significant, where we note increased lateral resolution of the channel system.

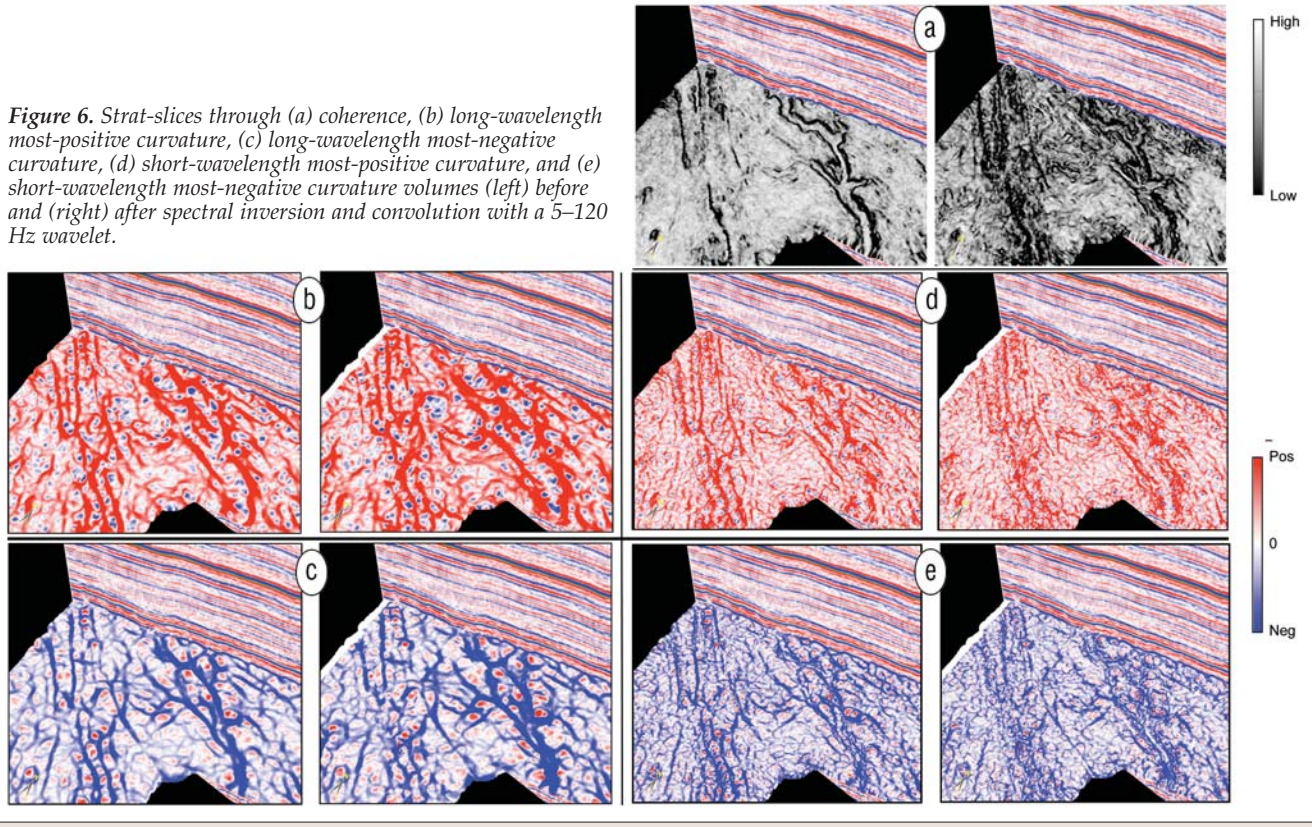


***Figure 6.*** *Strat-slices through (a) coherence, (b) long-wavelength most-positive curvature, (c) long-wavelength most-negative curvature, (d) short-wavelength most-positive curvature, and (e) short-wavelength most-negative curvature volumes (left) before and (right) after spectral inversion and convolution with a 5–120 Hz wavelet.*

**Volumetric computation of curvature.** Horizon-based curvature has been successfully used to predict faults and fractures, and shown to be correlated with open fractures measured on outcrops (Lisle, 1994) or measured by production tests (Hart et al., 2002). Horizon-based curvature is limited not only by the interpreter's ability to pick, but also by the existence of horizons of interest at the appropriate level in 3D seismic data volumes. Horizon picking can be challenging in data sets contaminated with noise and where rock interfaces do not exhibit a consistent impedance contrast amenable to human interpretation. The trend now is to use volumetric computation of curvature, which dispels the need for consistent horizons in the zone of interest (Al-Dossary and Marfurt, 2006). By first estimating the volumetric reflector dip and azimuth that represent the best single dip for each sample in the volume, followed by computation of curvature from adjacent measures of dip and azimuth, a full 3D volume of curvature values is produced. Many curvature measures can be computed, but the most-positive and most-negative curvature measures are perhaps the most useful in that they tend to be most easily related to geologic structures. Volumetric curvature attributes are valuable in mapping subtle flexures and folds associated with fractures in deformed strata. In addition to faults and fractures, stratigraphic features such as levees and bars as well as diagenetic features such as karst collapse and hydrothermally-altered dolomites also appear well-defined on curvature displays. Channels appear when differential compaction has taken place.

Multispectral curvature computation provides both long wavelength and short wavelength curvature estimates, which enhance geologic features having different scales. Curvature images having different wavelengths provide different perspectives of the same geology (Bergbauer et al., 2003). Tight (short-wavelength) curvature often delineates details within intense, highly localized fracture systems. Broad (long wavelength) curvature often enhances subtle flexures on the scale of 100–200 traces that are difficult to see in conventional seismic, but are often correlated to fracture zones that are below seismic resolution, as well as to collapse features and diagenetic alterations that result in broader bowls.

Figure 7 shows a time-structure map at 1600 ms interpreted from a 3D seismic volume acquired in Alberta, Canada. The horizon surface was manually picked on a 10 × 10 grid, autopicked, and smoothed using a 3 × 3 mean filter, which was then used to generate the horizon-based curvature images shown in Figures 7b and 7c. Notice that both displays are contaminated by acquisition footprint patterns (green ellipses). These types of overprints are artifacts and do not make any geologic sense. Horizons picked on noisy seismic data contaminated with acquisition footprint, or when picked through regions where no consistent impedance contrast exists (such as channels, turbidites, mass transport complexes and karst) can lead to inferior curvature measures. In spite of 3 × 3 spatial mean filtering, the horizon-based curvature estimates still suffer from artifacts. Figures 7d and 7e show volumetric most-positive and most-negative curvature attributes extracted along the picked-horizon surface in Figure 7a. These displays are free of the acquisition footprint artifacts in 7b and 7c.

In Figure 8, we depict strat-cube displays through volumetric estimates of coherence, most-positive and most-negative estimates of curvature. A strat-cube is a subvolume of seismic data or its attributes, either bounded by two horizons which may not necessarily be parallel or covering seismic data above/or below a given horizon. Notice the clarity with which most of the NS faults stand out on the coherence display; however, there is more fault fracture detail on the most-positive and most-negative curvature displays. The lineaments in red seen on the most-positive curvature display will correlate with the upthrown signatures that one would

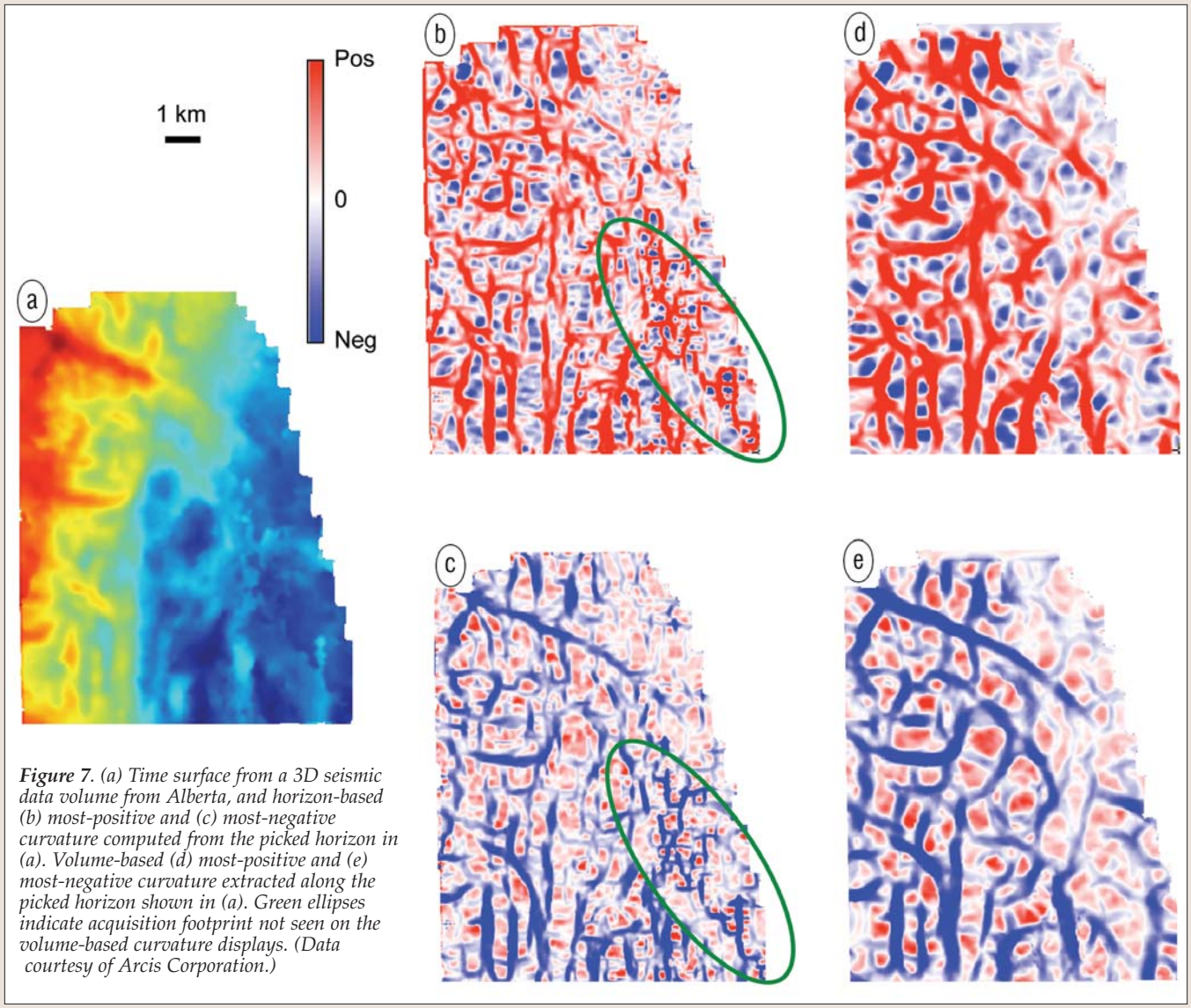


***Figure 7**. (a) Time surface from a 3D seismic data volume from Alberta, and horizon-based (b) most-positive and (c) most-negative curvature computed from the picked horizon in (a). Volume-based (d) most-positive and (e) most-negative curvature extracted along the picked horizon shown in (a). Green ellipses indicate acquisition footprint not seen on the volume-based curvature displays. (Data courtesy of Arcis Corporation.)*

see on the seismic. Similarly, the lineaments in blue seen on the most-negative curvature display will correlate with the downthrown signatures.

Not only faults and fractures, but stratigraphic features are often well-defined on volumetric curvature displays. Figure 9 shows strat-cube displays through coherence (Figure 9a), most-positive curvature (Figure 9b) and most-negative curvature (Figure 9c). Notice the clarity with which the channel features stand out on the curvature displays. Figure 10 shows strat-cube-seismic chair displays from (a) seismic amplitude, (b) coherence, (c) most-positive curvature (long-wavelength), (d) most-negative curvature (long wavelength), (e) most-positive curvature (short-wavelength), and (f) most-negative curvature (short wavelength). Notice, the top surface, which corresponds to a prominent horizon on the seismic, looks featureless on both the seismic as well as coherence images. However, the most-positive and most-negative curvature displays indicate fault features that can be directly correlated to the vertical seismic. The short-wavelength curvature displays show the fault features as crisp and clear.

**Attribute analysis of azimuth-limited seismic volumes.** Aligned subsurface vertical faults and fractures as well as nonuniform ambient stress cause azimuthal variations in seismic properties. 3D land surveys are usually acquired in such a way that (unknown) subsurface features are illuminated at as many directions as possible, giving rise to a high-fold full-azimuth survey. Conventional processing of seismic data typically stacks all azimuths together, thereby obliterating the azimuthal variation of amplitude and moveout. In order to better illuminate subtle faults and fractures, Chopra et al. (2000) present a method which first sorts the data into azimuthal bins based on the angle between sources and receivers on the Earth's surface. If the subsurface is isotropic, faults and fractures are best imaged by the azimuths perpendicular to them. Figure 11a, a time slice from a 3D OBC seismic coherence volume from West Africa, shows some NE–SW faults that are somewhat smeared. Missing on this display is a N–S fault which, based on production data, was expected to appear.

After application of zero-phase deconvolution in processing, the data were sorted into azimuth bins of 22.5°–67.5°, 67.5°–112.5°, 112.5°–157.5°, and 157.5°–202.5°. Subsequently, each volume was processed independently (through migration,) followed by running the coherence attribute. The bottom of Figure 11 shows time slices corresponding to the all-azimuth time slice shown in Figure 11a. Notice that different azimuth coherence slices show better alignment not only NE-SW but in orthogonal directions. A distinct cross fault (indicated by the green arrow) is seen on the E–W azimuth volume where it was expected. This methodology intuitively exploits the azimuthal variation of the P-wave

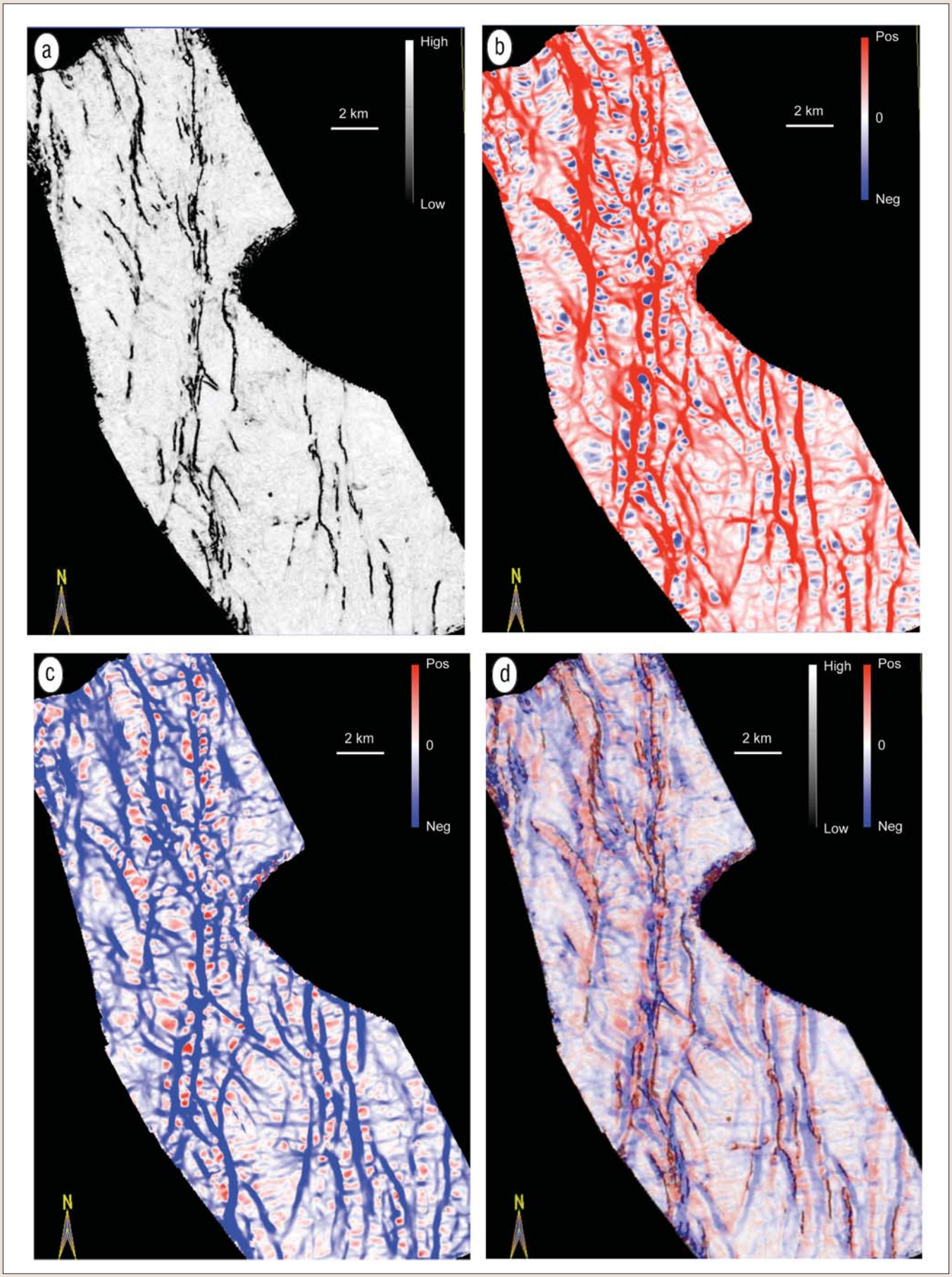


***Figure 8.*** *Strat cubes through (a) coherence, and long-wavelength (b) most-positive, and (c) most-negative attribute volumes. (d) Color stack of all three attributes. While some N–S faults are seen on the coherence display, the level of detail is much higher on the curvature displays. (Data courtesy of Arcis Corporation.)*

seismic signal to image subtle faults/fractures perpendicular to their travel path. A necessary requirement is that the input limited-azimuth volumes have sufficient (>12) fold in order to have a sufficient signal-to-noise ratio. While improved delineation of faults and fractures were obtained in this OBC example from West Africa and others from Alberta, azimuthally-limited volumes do not always result in higher resolution attribute images.

Perez and Marfurt (2007) observe that if there is significant azimuthal anisotropy, scattered energy sorted by surface source-receiver azimuth would still be smeared. They introduce bins that take into account the azimuth of the travel paths to the image point from the surface source and receiver. Migration with this approach images data into azimuths that more accurately represent the direction of propagation. Discrimination into separate orientations in the azimuth domain results in increased resolution of perpendicular geologic features.

Volumetric attributes such as coherence and curvature run on azimuth-limited images based on this approach result in improved detection and better resolution of faults and associated fractures. Figure 12a from the Fort Worth Basin, Texas, shows time slices at 1.36 s through a most-negative curvature volume computed from an azimuth-limited partial stack using conventional

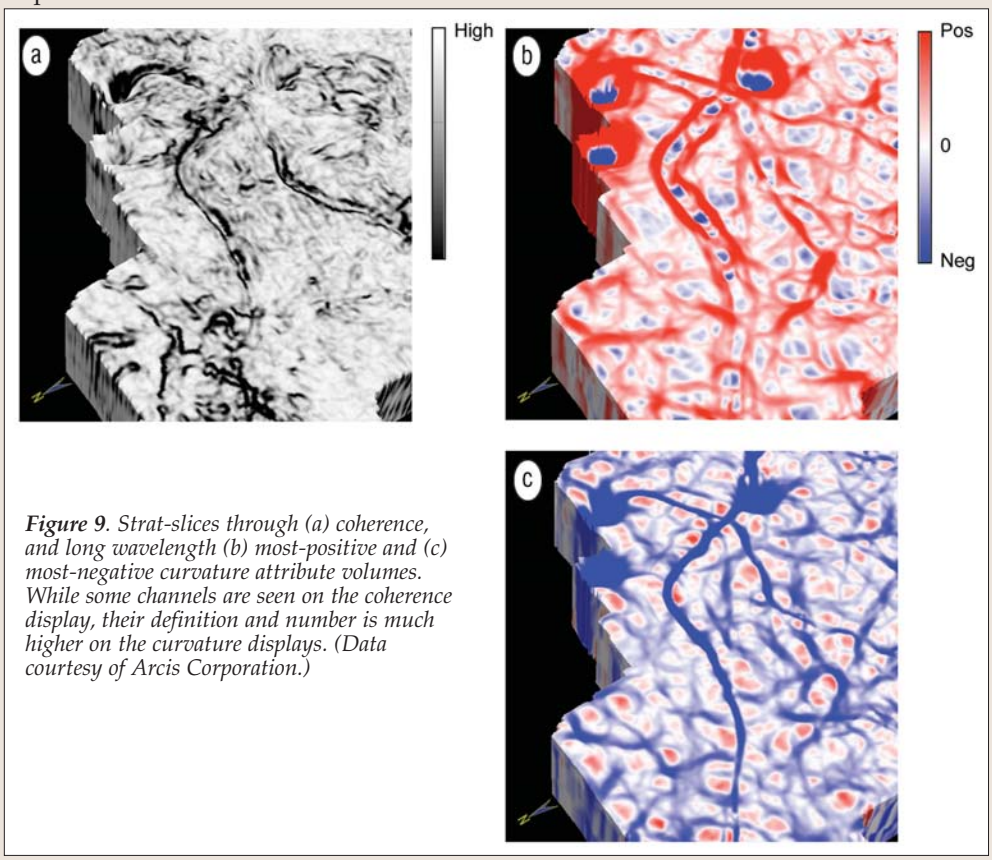


***Figure 9**. Strat-slices through (a) coherence, and long wavelength (b) most-positive and (c) most-negative curvature attribute volumes. While some channels are seen on the coherence display, their definition and number is much higher on the curvature displays. (Data courtesy of Arcis Corporation.)*

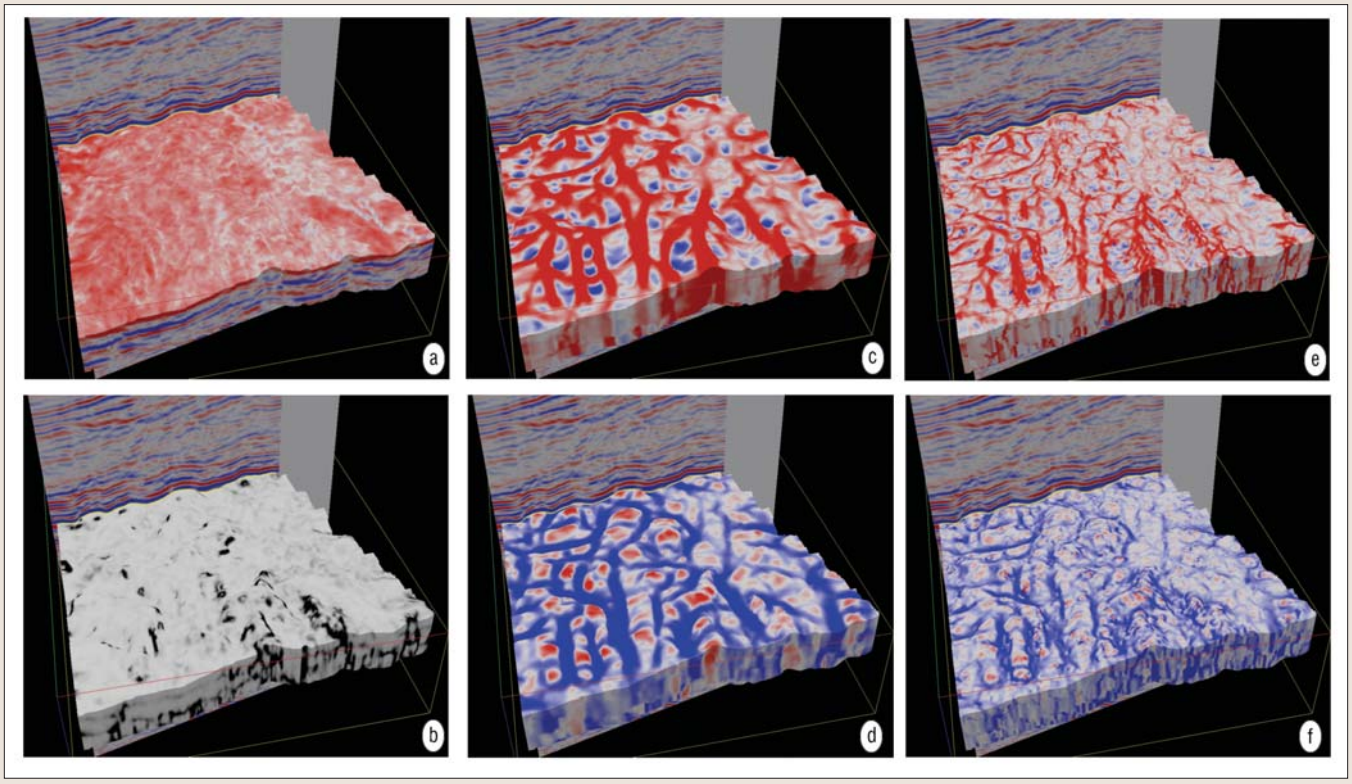


***Figure 10.** Zoom of chair displays in which the vertical display is an inline from the 3D seismic volume and the horizontal displays are strat-slices through (a) the seismic (b) coherence, long-wavelength (c) most-positive and (d) most-negative curvature, and short wavelength, (e) most-positive and (f) most-negative curvature attribute volumes. The fault lineaments correlate with the upthrown and downthrown signatures on the seismic.(Data courtesy of Arcis Corporation.)*

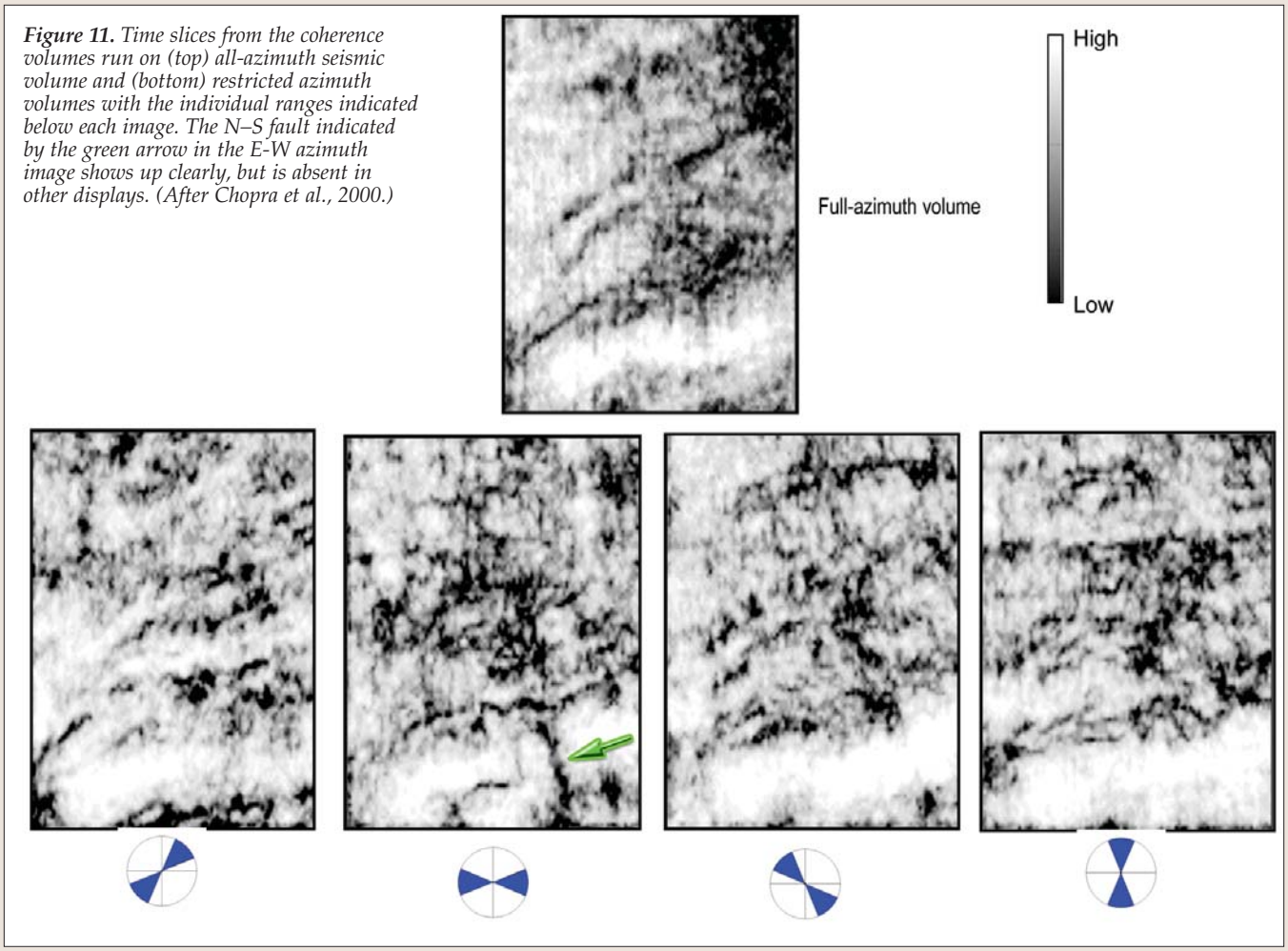


***Figure 11.*** *Time slices from the coherence volumes run on (top) all-azimuth seismic volume and (bottom) restricted azimuth volumes with the individual ranges indicated below each image. The N–S fault indicated by the green arrow in the E-W azimuth image shows up clearly, but is absent in other displays. (After Chopra et al., 2000.)*

azimuth binning. Figure 12b shows the corresponding result obtained with the modified binning. Arrows indicate subtle faults and flexures that are better resolved using the modified binning method that takes into account the azimuth of the travel path to the image point during migration.

**Attribute visualization and display**. Early attempts at 3D visualization began with inline, crossline, time- and horizon-slice animations by highly technical geophysicists using expensive, specialized computer hardware. Advances in hardware and software have brought volume rendering, geobody tracking, and visualization, as well as virtual realization to every interpreter's desktop. Similar advances allow us to render multiple attribute slices or subvolumes (including the original seismic) each with their own user-defined color bar (Figure 13). The interactive use of color adjustment, direction of

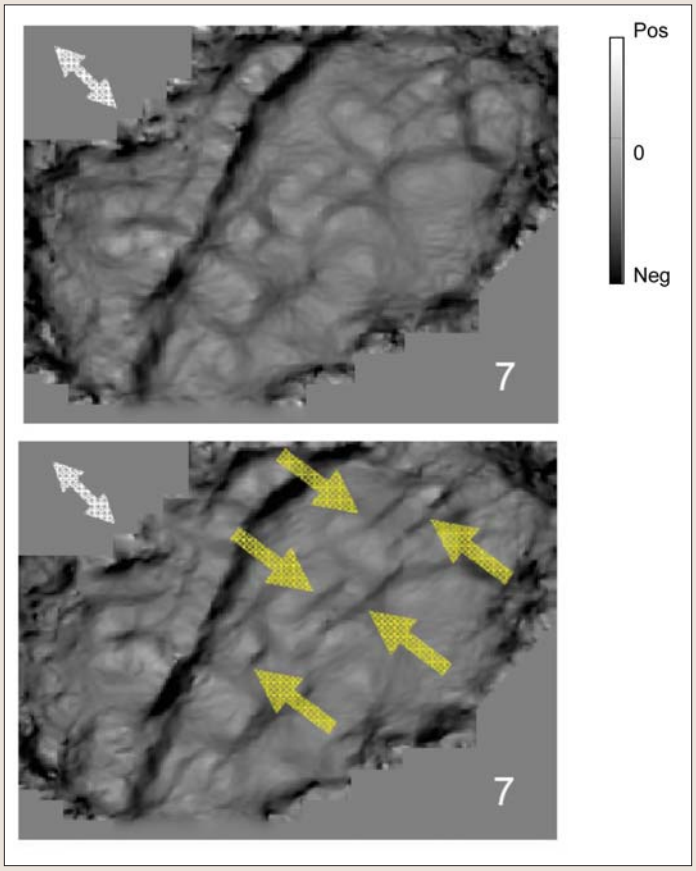


***Figure 12.*** *Time slices at 1.36 s through most-negative curvature volumes computed from (a) azimuth-limited partial stacks using conventional azimuthal binning and (b) modified azimuthal binning. The best imaged features strike approximately at right angles to the corresponding azimuthal orientation. For instance, large-curvature zones approximately oriented SW–NE (indicated by the yellow arrows in the corresponding image) are best seen at SE–NW azimuths.*

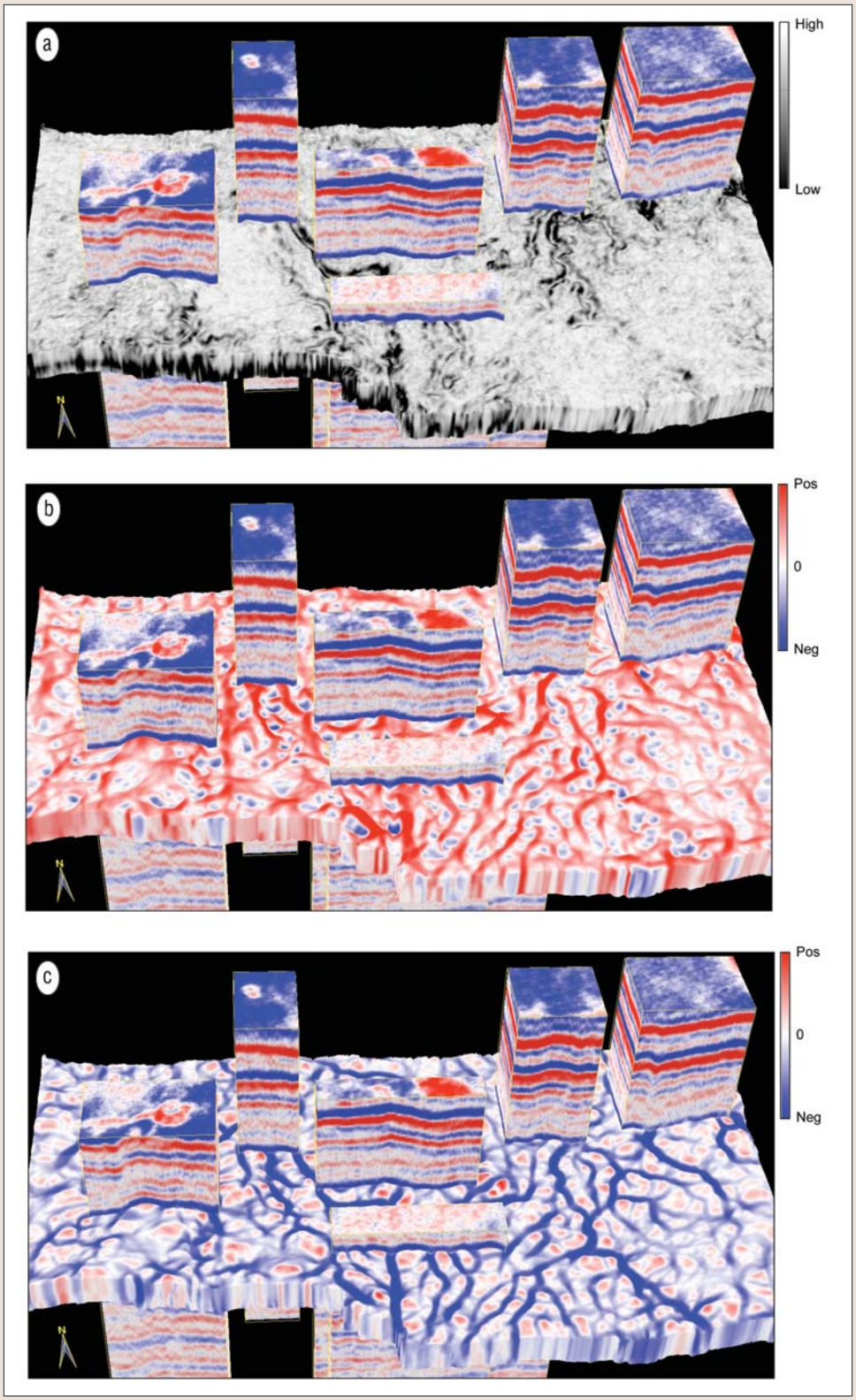


***Figure 13.*** *Covisualization of seismic subvolumes and strat cubes from (a) coherence (b) most-positive and (c) most-negative curvature volumes. Several channels are seen on the coherence strat cube, but a more complete system is seen on the most-negative curvature (which delineates the channel axes, or thalwegs) and most-positive curvature (which delineates the channel flanks). (Data courtesy of Arcis Corporation.)*

lighting, and opacity allows the interpreter to highlight subtle stratigraphic detail that otherwise could be missed.

All commercial workstations have the ability to plot a single seismic or attribute volume against 256 discrete colors displayed as single gradational, dual gradational, or cyclical 1D color bars. Most workstations allow the interpreter to modulate this color bar with a 1D opacity control, thereby enhancing 3D volumetric views of voxels whose values fall with a user-defined range. Modern workstations also allow the visualization of multiple attribute vertical, time, horizon, or stratal slices, as well as subvolumes, in the same image, each with its own unique color bar. We demonstrate this capability in Figure 13, where we corender stratal slices through coherence, most-positive curvature, and most-negative curvature with several seismic subvolumes. Such co-rendering capabilities are key to visually calibrating geomorphological features and structural lineaments seen on stratal and horizon slices with the seismic amplitude signature seen on vertical slices to ascertain whether the features are indeed geologic, or a seismic acquisition or processing artifact. The interpreter can interactively rotate the volume display in any direction to better understand the data disposition.

Several workstation implementations allow the interpreter to plot different attributes against red, green, and blue primary colors. Guo et al. (2008) find that this color model works best when attributes are of similar type, such as near-, mid-, and far-offset seismic amplitudes. Giroldi and Alegria (2005) use the RGB color model to plot spectral components of 20, 25, and 30 Hz to generate the composite image in Figure 14. A system of channels, clearly seen on the multiattribute spectral decomposition image, are difficult to see on the rms amplitude image even though both extractions were made using the same time interval and calculated with an equivalent window size.

Guo et al. show how the hue-lightness-saturation (HLS) color model can be constructed to display a second or third attribute. The HLS color bar is displayed alternatively as a three-axis dual pyramid, sphere, or cylinder developed by Munsell early in the twentieth century and shown in Figure 15. While Rijks and Jauffred (1991) used a 2D hue-lightness color bar over 15 years ago, such capabilities were not available in commercial software until the introduction of "attribute cal-

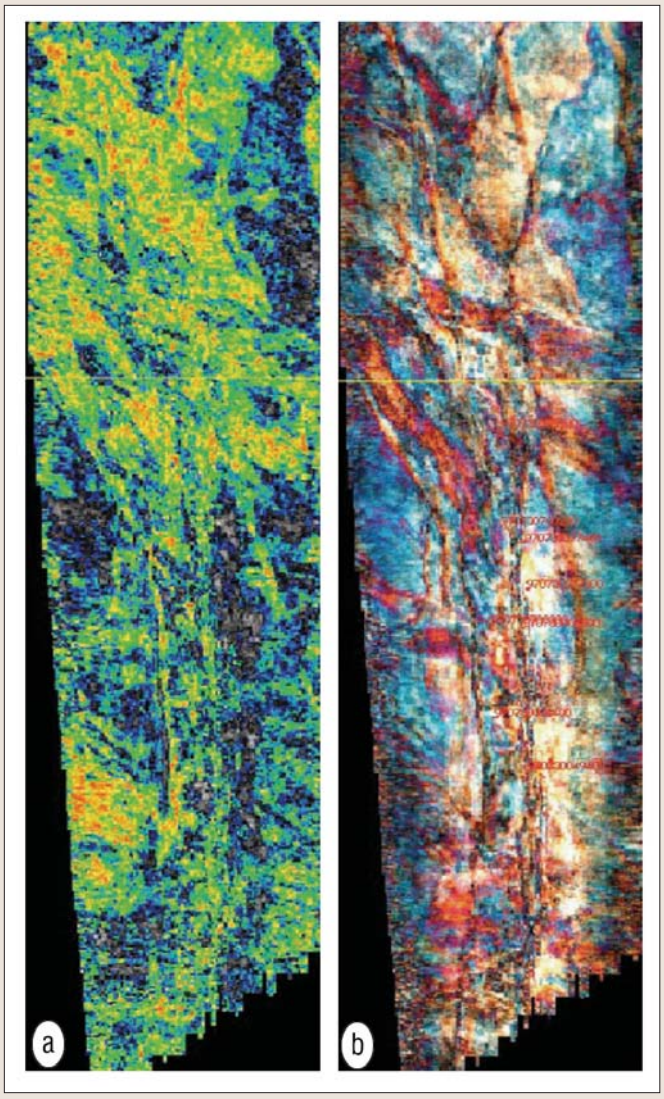


***Figure 14.*** *(a) Conventional poststack rms amplitude extraction at a given level in the analysis window. (b) A composite spectral decomposition image with spectral magnitude at 20, 25, and 30 Hz plotted against red, green, and blue color components to form a color stack. While the same overall picture of the channels emerges, the spectral decomposition image is much crisper and richer in detail. (After Giroldi and Alegria, 2005).*

culators"discussed below. Figure 16 shows peak spectral amplitude against lightness and peak spectral frequency against hue using such an attribute calculator. Carlson and Peloso (2007) use hue, lightness, saturation, and opacity to display four attributes (Figure 17).

Advances have been made in not only the quantity and variety of data that can be corendered but in the flexibility in which geoscientists can extract the most relevant information using an optimized visual perspective (Roth et al., 2005). Wallet and Marfurt (2008) use similar interpreter-driven projections in their analysis of spectral components discussed in a companion paper in this issue.

**Texture attributes**. By construction, geometric attributes measure lateral variation in reflector amplitude, phase, and waveform using a well-defined and easily understood model. Thus dip and azimuth measure the lateral change in phase (traveltime) while curvature measures lateral changes in dip and azimuth (second derivatives of traveltime). Spectral and other decomposition algorithms (such

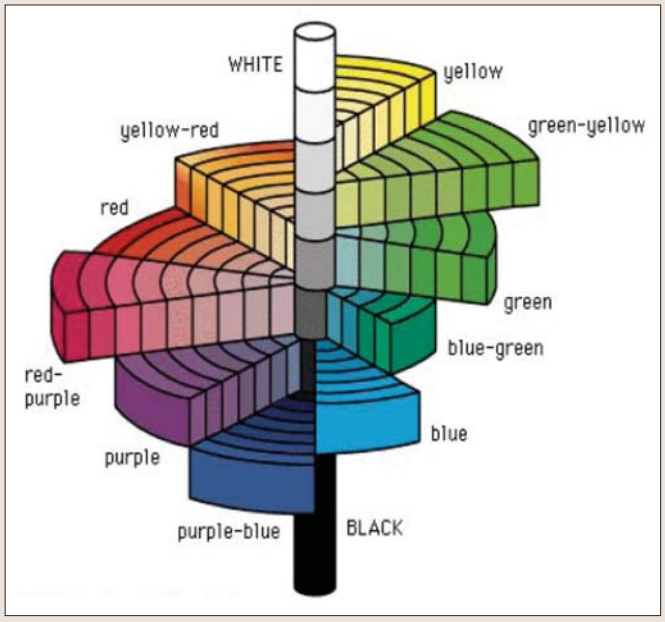


***Figure 15.*** *Munsell's color cylinder. Circumferential axis is hue, or color wavelength. Radial axis is saturation or the degree color differs from gray. Vertical axis is lightness (also called value), or brightness of color. (After Carlson and Peloso, 2007).*

as those based on Chebyshev polynomials) crosscorrelate each trace against a suite of precomputed standard waveform. The interpreter then examines the crosscorrelation coefficients (what we commonly call spectral components) in map view, and interprets the observed patterns using concepts of seismic geomorphology and thin-bed tuning.

*Waveform classification*. An alternative to using predefined sine and cosine waveforms is to compute waveforms that best represent the amplitude variation seen about the interpreted horizon. Several alternative clustering algorithms are available, but the current method of choice is that of self-organizing maps. Originally, the interpreter needs to guess at how many clusters were needed to represent the data. Clever mapping of the color spectrum against the ordered suite of clusters minimizes errors in making an inaccurate guess (for example, with too many clusters resulting in an extra "indigo"cluster falling between the "blue"and "violet"clusters). More recently, Strecker et al. (2005) plotted 2D self-organized maps against a 2D color bar, resulting in images that look significantly more geological than earlier 1D clustering plotted against a 1D color bar. Matos et al. (2007) show that by using a large number of prototype clusters, the optimum number of clusters can be estimated by means of a U-matrix and other statistical measures. Such waveform classification has proven a very popular interpretation tool, with the results interpreted in the context of seismic geomorphology, and correlating seismic facies to clusters through a combination of direct well control, or through pseudo-well analysis using fluid substitution, and lithology perturbation followed by careful generation of synthetics.

*Waveform fragmentation.* Carlson and Peloso (2007) find statistical analysis of seismic waveform lobes to be a powerful alternative to waveform classification and spectral decomposition. Waveform lobes are defined as falling between zero crossings. Each lobe is then represented by four attributes or measures: peak amplitude, shape (symmetrical, top-loaded, or bottom-loaded) thickness, and string-length ratio (a measure of complexity).

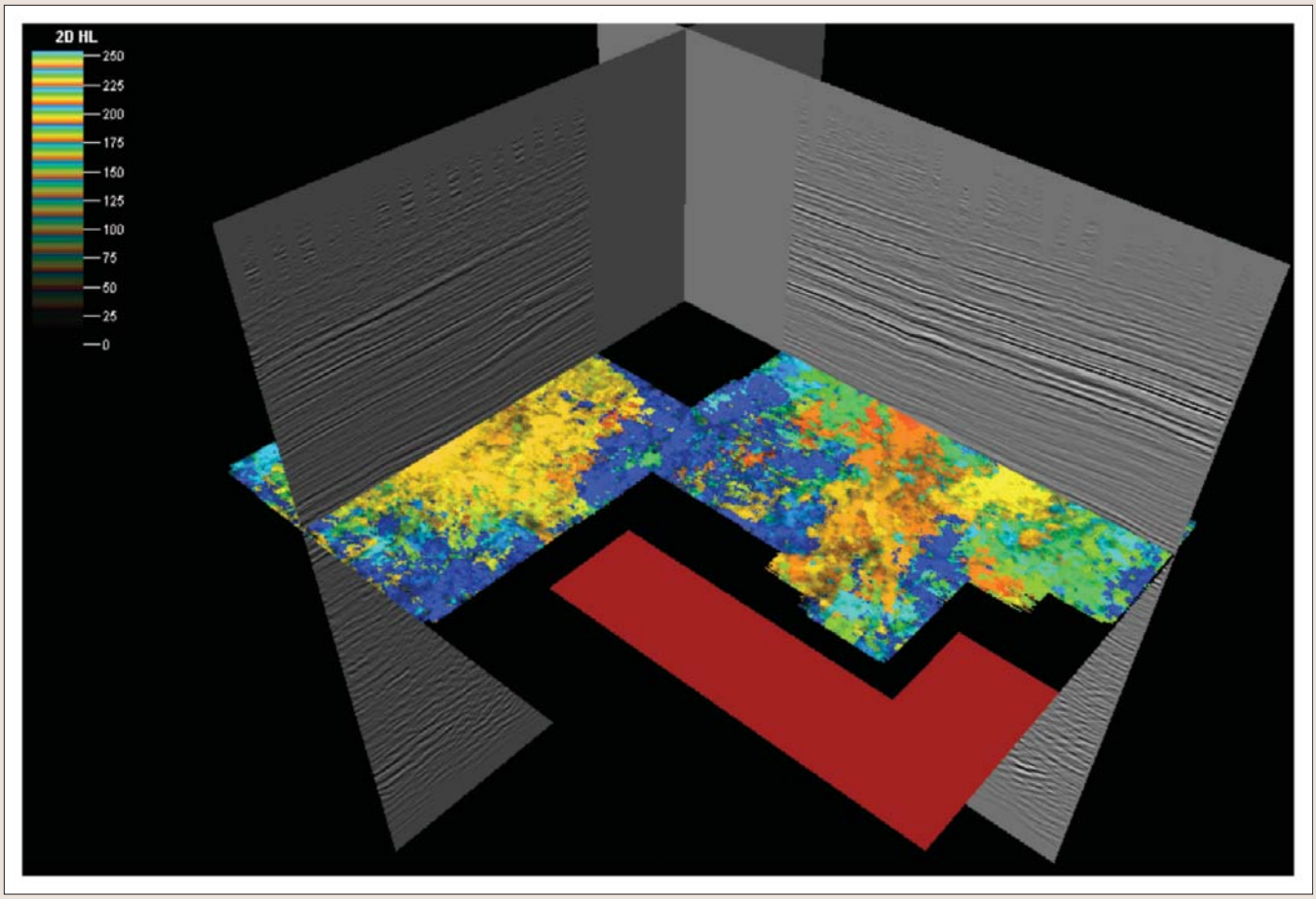


***Figure 16.*** *An example of 2D color display using an "attribute calculator"in a commercial workstation. In this example we combine two attributes into a single output attribute whose values range between 0 and 255. Each value is associated with a color in a 2D color table. Attributes are peak spectral amplitude and frequency at peak spectral amplitude. These colors allow the interpreter to read off the tuning thickness of strong events.*

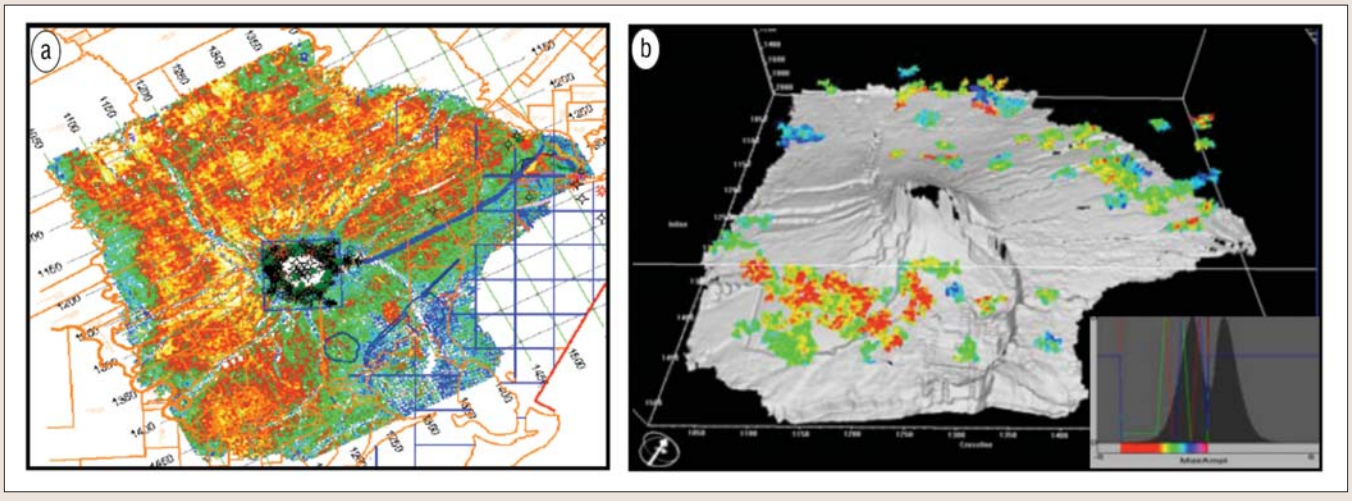


***Figure 17.*** *(a) Amplitude map of a productive hydrocarbon zone over a salt dome. (b) 3D display of extracted geobodies having the calibrated signature. Overlain color is the maximum amplitude, with high-negative amplitudes in red. (After Carlson and Peloso, 2007).*

Figure 17 shows an example over an onshore US Gulf Coast salt dome. The amplitude distribution corresponding to the production level shows high negative amplitudes over a large area, which makes it difficult to determine the location of pockets that are more prospective then others. After fragmentation analysis, the four attributes are mapped into hue-lightness-saturation-opacity space in the visualizer, with each attribute displayed according to the observed range of values in the data. Next, all voxels visually having the four attributes within an interpreter-defined cutoff range are extracted and connected into geobodies. Figure 17b shows such extracted geobodies, which may lie above or below the prospective reflector in Figure 17a. This method yields geobodies that show more details than those created

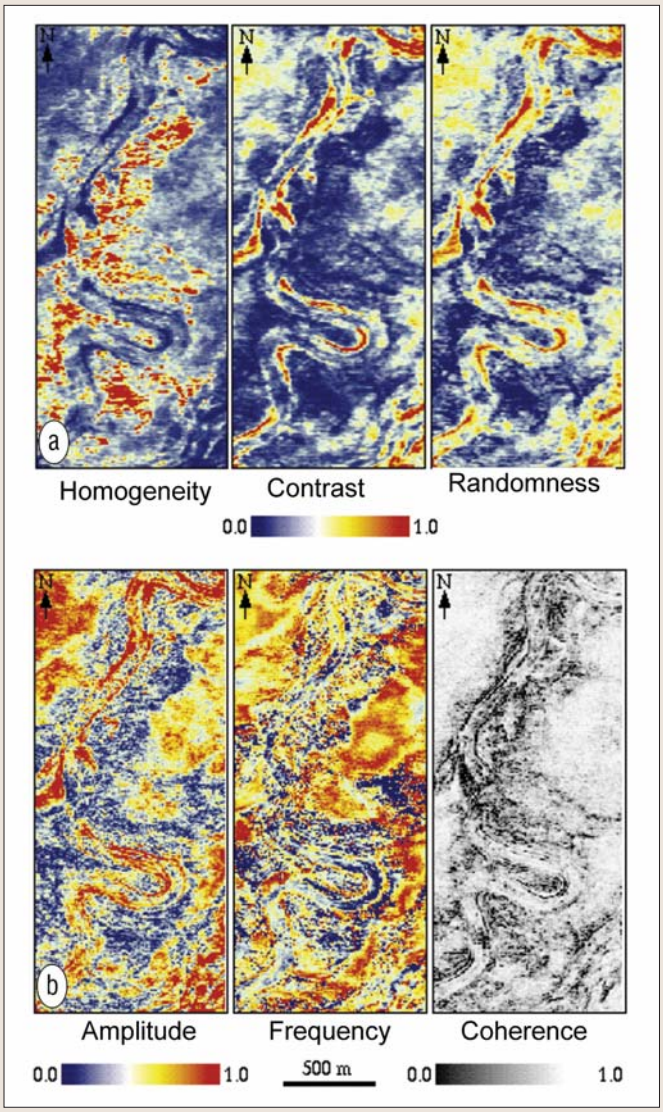


***Figure 18.*** *Comparison between textural attributes and conventional seismic attributes in map view at a stratigraphic level in the upper Miocene interval. Both conventional and textural attribute sets are derived from the same 3D seismic data set at the same stratigraphic level by using the same processing parameter (Figure courtesy of Dengliang Gao.)*

with single attributes.

*Statistical measures of texture.* Not all seismic features can be easily defined by a simple vertical or lateral change in amplitude and phase, giving rise to statistical rather than deterministic attributes. The simplest, oldest, and perhaps most commonly used statistical attribute is rms amplitude which simply computes the root-mean-square amplitude of the trace within a user-defined window. Generalizing this 1D single-trace measure to a small 3D window of traces and samples gives rise to what are commonly called texture attributes. The human brain is very proficient at recognizing textures. Skilled interpreters correlate textures that look like smiles and frowns to migration artifacts and textures that look like the wings of a seagull to channel-levee complexes. Sometimes seismic features are described as shingled, hummocky, wormy, or even ratty. Amalgamated channels, karst, turbidites, mass transport complexes, and diagenetically-altered dolomites all have distinct textures and cannot be defined by simply mapping peaks and troughs. Considerable progress has been made in 3D statistical measures of seismic amplitude and phase, giving rise to what are called "texture attributes."

Most present-day texture attributes are based on the gray level co-occurrence (GLCM) matrix. The commonly used texture measures are energy (a measure of textural uniformity), entropy (a measure of disorder or complexity), contrast (a measure of local variation) and homogeneity (a measure of overall smoothness). When applied to seismic data, high-amplitude continuous reflections generally associated with marine shale deposits have relatively low energy, high contrast and low entropy (Gao, 2003). Low-amplitude discontinuous reflections generally associated with massive sand or turbidite deposits have high energy, low contrast, and high entropy. Low-frequency high-amplitude anomalies generally indicative of hydrocarbon accumulations generally exhibit high energy, low contrast, and low entropy relative to nonhydrocarbon sediments. Figure 18 compares three textural attributes (homogeneity, contrast, and randomness) and three more conventional attributes (amplitude, instantaneous frequency, and coherence). Notice the textural attributes are superior to conventional attributes in terms of resolution, sensitivity, and significance to facies variations. West et al. (2002) computed such GLCM-matrix-based textures to train a neural network to imitate an experienced seismic interpreter.

*Seismic morphological imaging.* Morphologic attributes like size, orientation, geometric complexity (such as linear versus meandering versus anastomosing), and planar curvature (describing scroll bars in fluvial-deltaic depositional environments) can quantify different morphological features. A supervised neural network can be used to correlate these morphological attributes to facies classes. The supervised learning phase comprises converting sample depositional facies into facies categories labeled by arbitrary numbers (1, 2, 3,...etc). After satisfactory training and validation, the full seismic volume can be transformed into a depositional facies volume.

Another statistical pattern recognition technology traces its origins to biological sciences and was introduced to the industry by Durham (2001). This technology does not require any neural network type of training phase but operates directly on the seismic data to yield information on stratigraphy or isolate those regions in the data that may be geologically promising. This technology can quickly "mine"seismic data for exploration leads.

*User-defined volume-attribute calculators.* Several commercial workstation software packages now allow interpreters to define/generate their own attributes from seismic or attribute data volumes and/or from picked surfaces and horizon attribute extractions. While slower to run than a compiled program, this development allows any interpreter whose programming skills are not much beyond that of filling out a spreadsheet to develop innovative workflows. Figure 16 shows an example of displaying peak spectral amplitude and frequency at the peak spectral amplitude in a single image via the formula using a 2D hue-lightness color bar described by Guo and Marfurt (2008):

*amp_freq_output=MIN(ROUND((peak_amp_input_Realized-peak_amp_input_Realized.min) /((peak_amp_input_Realized.max-peak_amp_input_Realized.min)/15)),15)*16+ MAX(MIN(ROUND((peak_freq_input_Realized-peak_freq_input_Realized.min) /(peak_freq_input_Realized.max-peak_freq_input_Realized.min)*15),15),0)*

where

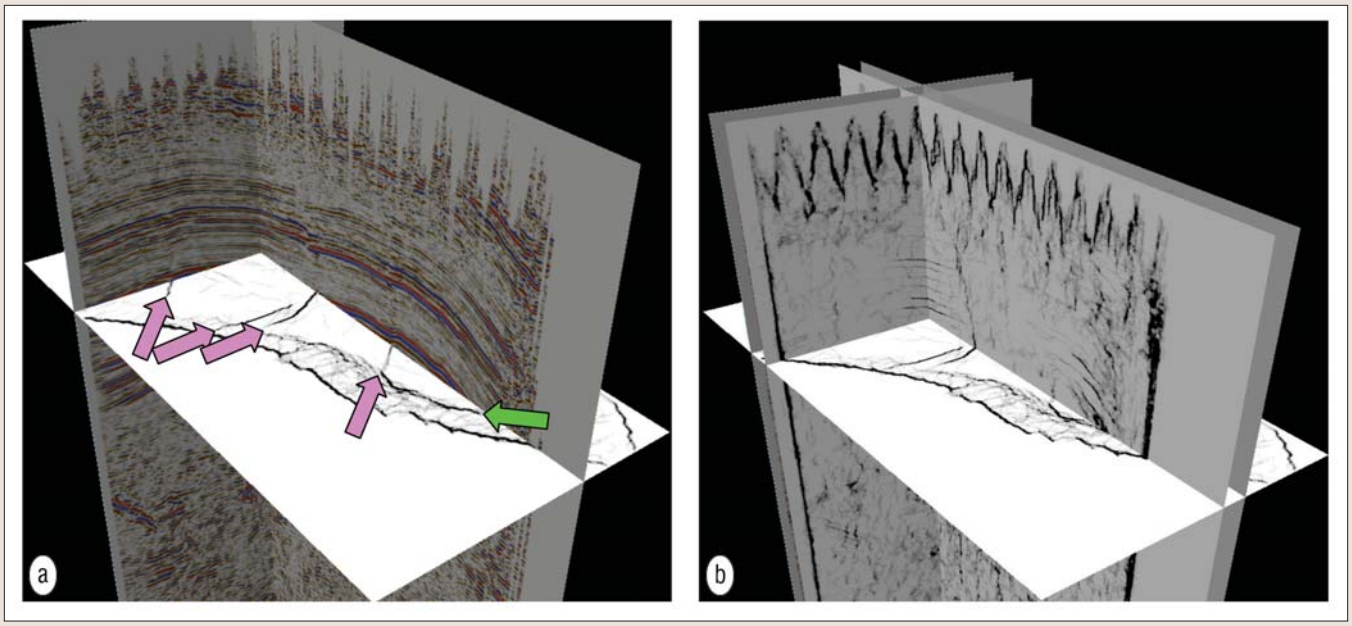


***Figure 19.*** *The result of ant-tracking applied to a coherence volume computed over Teapot Dome, Wyoming. The ant-tracker does a very good job of delineating the major faults (magenta arrows) but has no way to know that the low coherence event indicated by the green arrow is an artifact due to steep dip (seen in (a) and (b).) (Figure courtesy of Rocky Mountain Oilfield Technology Center.)*

*amp_freq_output* is the name of the output data volume whose values range between 0 and 255,

*peak_amp_input_Realized* is the input peak amplitude volume stored in brick format (or "realized" in the particular software package used),

*peak_freq_input_Realized* is the input peak frequency volume stored in brick format,

the suffixes '.min' and '.max' denote the minimum and maximum values of the specific volume,

*ROUND* is a function that rounds a floating point number to the nearest integer (thereby placing it into a specific hue or lightness color bin),

*MIN* and *MAX* clip the 2D color axes to fall between 0 and 15,

and the 2D color bar consists of 16 hues and 16 lightnesses giving a total of 256 colors.

Similar formulae can be generated to plot three attributes against a 3D color bar or to apply logic where, for example, coherence is plotted if the value of coherence is low, while envelope is plotted otherwise, such as described by Chopra (2002) using processing rather than interpretation software. For compartmentalized reservoirs, geometric attributes (indicating faults/fractures) can be combined with oil and gas indicators (envelope, impedance or AVO anomaly indicators).

*Image processing for automatic fault detection.* Faults control both reservoir compartmentalization and internal plumbing. Fault interpretation on 3D seismic data volumes is very subjective and labor-intensive. Such manual interpretation is most commonly performed on time slices and vertical slices parallel to the fault strike. Coherence, curvature, and other attributes sensitive to faults can greatly accelerate this process by providing images of the fault network and, implicitly, the fault hierarchy. However, converting these images into computer fault plane "objects"is still carried out by explicitly picking fault segments on either time or vertical slices which are subsequently joined together to form a fault surface. During the past 3–5 years, automated attribute-assisted fault object generation algorithms have been deployed to commercial workstations. While 3D generalizations of 2D Hough transforms have been successfully demonstrated to enhance faults (AlBinHassan and Marfurt, 2003; Jacquemin and Mallet, 2005), such algorithms have not made it into the interpretation workstation marketplace. Rather, iterative workflows that address nonfault features such as stratigraphically-aligned discontinuities and acquisition footprint appear the most promising practical tools.

Barnes (2005) starts with a coherence image and then exploits several well-established image-processing techniques. First, he suppresses low-coherence geological (such as mass transport complexes and condensed sections) or geophysical (such as zones where the background noise overwhelms the amplitude of a weak reflector) features that parallel stratigraphy, and enhances steeply dipping features (such as faults) through a suite of simple filters. The result of such filters is a collection of mostly disconnected steeply dipping patches. Next, he "dilates" these patches such that as they grow longer, wider, and fatter, they connect to each other. Dilation is followed by "image erosion" to generate a surface that is only one pixel thick. This skeletonized, fault-enhanced version of coherence can then be either optically corendered with the original seismic, or digitized using an autopicker.

Dorn et al. (2005) present another workflow in which the first step is a classical destriping operator applied to time or depth slices to remove any remnant acquisition footprint. Once the linear artifacts are suppressed, linear low-coherence features (that we hope are associated with faults) are examined to see if they can be linked to form a longer line segment. The result is a relative probability volume, where each sample represents the relative probability that it belongs to a horizontal linear feature. Filters can be applied to restrict the azimuth range or exclude linear features less than a user-defined length. The line-enhanced volume is next subjected to a fault enhancement process whereby linear features having the same azimuth are now linked in time or depth. Vertically-limited linear features corresponding to channel boundaries, pinchouts, and unconformities are filtered out at this step.

The ant-tracking algorithm (Randen et al., 2002) is an iter-

ative scheme that progressively tries to connect adjacent zones of low coherence that have first been filtered to eliminate horizontal features associated with stratigraphy. The ant tracking algorithm draws an analogy from ants finding the shortest distance between their nest and their food source, and communicating by making use of chemical substances called pheromones, which attract other ants. Ants following the shortest path will reach their destination earlier and so other ants are influenced by the pheromone on the traversed path. The shorter path will thus be more and marked with pheromone.

In the software implementation, artificial electronic ants are distributed in the seismic coherence attribute volume and allowed to follow different paths. Ants following a fault will trace the fault surface for a specific distance before it fades out. Ants deployed at different positions in the coherence volume will traverse the fault surface and mark it with pheromones. In contrast surfaces that do not represent faults will be weakly marked and can be removed by setting a subsequent threshold filter. As these ants traverse different surfaces in the coherence volume, they also estimate the orientation of these surfaces, with both the attribute strength and orientation stored at each sample. These two measures permit construction of fault objects. Like the two previous methodologies, filters can be applied to reject small patches, and objects that have dips and azimuths that can be attributed to either acquisition footprint or stratigraphic features.

All three of these algorithms (and others that are commercially available but not described in the scientific literature) are only as good as the attributes they act upon. Figure 19 shows ant-tracking applied to a coherence attribute computed from a survey over Teapot Dome, Wyoming. The delineation of the faults indicated by the magenta arrows is excellent. However, the ant tracking also "picks"a coherence artifact associated with steep dip (indicated by the green arrow).

**Future advances.** Seismic attribute technology will advance through improvements in seismic data acquisition and processing, through continued attribute calibration to well data and geologic models, and through continued algorithm development and interpretation workflows.

*Processing and acquisition.* While attributes are routinely applied to 3D seismic volumes, only recently have they been applied to common-offset and common-azimuth volumes. We predict a continued integration of volumetric attribute and AVO technology, with long-offset volumes delineating features associated with changes in shear-wave impedance and/or the presence of hydrocarbons.

Converted-wave volumes have become more economic following the introduction of high-fidelity multicomponent piezoelectric geophones. Four-component "shear wave"exploration is more economic following the introduction of simultaneous vibrator sweeps on separate source components. Thus, volumetric attributes will be applied to not only P-wave volumes, but to converted-wave, slow-shear, and fast-shear volumes. The authors have seen presentations where horizons on P-wave and S-wave sections are correlated through attribute-delineation of unique horizon-specific stratigraphic features. While converted- and shear-wave images are often of lower resolution than corresponding compressional-wave images, they are significantly more sensitive to changes in shear impedance than moderate-offset compressional waves, thereby illuminating lithologies and hydrocarbons differently.

As oil fields mature, time-lapse (4D) seismic is also becoming more common. Attributes applied to time-lapse images often show changes of the production front, particularly if the gas comes out of solution with decreasing pressure. In addition to showing production of fluids, such images can illuminate previously unresolveable faults, allowing engineers to identify by-passed pay.

Since they enhance subtle changes in amplitude and phase, attributes are particularly sensitive to errors (and enhancements) in processing. Since their inception, attributes such as coherence have been used to evaluate alternative processing flows and parameter choices. Attribute time-slice images are particularly valuable in evaluating the impact of processing choices on subtle stratigraphic and diagenetic features of interest that are difficult to see on vertical seismic. Recent developments in fracture illumination by Fomel et al. (2007) bridge the boundary between processing and attribute interpretation.

Several processing parameters are one and the same as seismic attributes. Thus, continuing advances in measuring seismic anisotropy and seismic attenuation will result in "attributes"that we can incorporate directly into our interpretation workflows.

*Calibration.* We predict continued efforts in seismic geomorphology beyond the current emphasis on fluvial-deltaic, deepwater turbidite, and carbonate systems to include analysis of fractured basement, volcanics, and diagenetically altered facies.

Workflows for correlating seismic attributes to map natural or artificially-induced fractures are still in the early stages of their application. While volumetric curvature attributes on poststack data are a great help to the interpreter, development of attributes sensitive to azimuthally-limited fracture sets and their applications will be seen in the near future. Calibration of such attributes with fracture-sensitive measurements including image logs, tracer data, production (flow) rates, and microseismic measurements will be seen more and more. Application of attributes to distinguishing between open and sealed fractures is in its infancy; we expect to see more attribute applications in this area.

Statistical pattern recognition techniques will be used more and more to automate the sifting of large quantities of data and observing target features, although the refinement of such techniques could take some time. More neural net applications using texture attributes could aid characterization of target reservoir zones. We predict continued advancement in computer-assisted 3D seismic stratigraphy, with algorithms able to delineate seismic stratigraphic textures including onlap, offlap, parallelism, sigmoidal features, and hummocky clinoforms in 3D.

*Algorithm development and workflows.* Crossplots of attributes have been used to identify and interpret seismic patterns associated with target zones, using polygons to capture the interesting parts of data clusters. This methodology is actively used in AVO analysis but has immense potential for application with other attributes. After performing principal component analysis on suitable attributes, attempts have been made at crossplotting the first and second principal components to distinguish favorable target zones which separate as clusters on 2D crossplots. This is one area we feel will be explored more in terms of 3D crossplotting using three different attributes characterizing patterns to identify seismic objects in 3D domain.

Just like the concept of textures was adapted from image processing, another promising concept is the "snake"algorithm. Snakes are active contour models that lock or terminate at local edges in an image segment, thereby localizing them accurately. Originally introduced by Kass et al. (1988), this algorithm is used for automated image segmentation.

When the edges of an image segment are not continuous, low-level image processing may not help and so an active contour algorithm (or snake) algorithm is used. By employing properties such as continuity and smoothness to the desired contour, the active contour also performs an accurate job. The snake algorithm and its different implementations have become a standard tool in medical image analysis. We expect such algorithms can be generalized to auto-track channels and other stratigraphic features in 3D.

**Suggested reading.** "Imaging of basement control of shallow deformation; application to Forth Worth Basin" by Aktepe and Marfurt (*SEG 2007 Expanded Abstracts*). "Acquisition footprint suppression via the truncated SVD technique: Case studies from Saudi Arabia" by Al-Bannagi et al. (*TLE*, 2005). "Fault detection using Hough transforms" by AlBinHassan and Marfurt (*SEG 2003 Expanded Abstracts*). "Multispectral estimates of reflector curvature and rotation" by Al-Dossary and Marfurt (GEOPHYSICS, 2006). "Improving curvature analyses of deformed horizons using scale-dependent filtering techniques" by Bergbauer et al. (AAPG *Bulletin*, 2003). "Volume-based curvature analysis illuminates fracture orientations" by Blumentritt (AAPG 2006 Annual Meeting). "Multi-attribute visual classification of continuous and fragmented seismic data" by Carlson and Peloso *(SEG 2007 Expanded Abstracts*). "Comparison of spectral decomposition methods" by Castagna and Sun (*First Break*, 2006). "Instantaneous spectral analysis: Detection of low-frequency shadows associated with hydrocarbons" by Castagna et al. (*TLE*, 2003). "High-frequency restoration of surface seismic data" by Chopra et al. (*TLE*, 2003). "Curvature attribute applications to 3D seismic data" by Chopra and Marfurt (*TLE*, 2007). "Seismic attributes for prospect identification and reservoir characterization" by Chopra and Marfurt (SEG CE Course, 2007). "Seismic attributes—A historical perspective" by Chopra and Marfurt (GEOPHYSICS, 2005). "Seismic resolution and thin-bed reflectivity inversion" by Chopra et al. (CSEG *Recorder*, 2006). "Practical aspects of curvature computations from seismic horizons" by Chopra et al. (*SEG 2006 Expanded Abstracts*). "Azimuth-based coherence for detecting faults and fractures" by Chopra et al. (*World Oil*, 2000). "2D stationary wavelet-based acquisition footprint suppression" by Cvetkovic et al. (SEG 2007 *Expanded Abstracts*). "Automatic fault extraction (AFE) in 3D seismic data" by Dorn et al. (CSEG 2005 National Convention). "Technology unravels 'Genetic Code' of 3D data to improve quality, speed of seismic exploration" by Duncan and Latkiewicz (*American Oil and Gas Reporter*, 2002). "Successful application of spectral decomposition technology toward drilling of a key offshore development well" by Fahmy et al. *(SEG 2005 Expanded Abstracts*). "Volume texture extraction for 3D seismic visualization and interpretation" by Gao (GEOPHYSICS, 2003). "Mapping multiple attributes to 3- and 4-component color models—A tutorial" by Guo et al. (GEOPHYSICS, 2008). "Using spectral decomposition to identify and characterize glacial valleys and fluvial channels within the carboniferous section in Bolivia" by Giroldi and Alegria (*TLE*, 2005). "Footprint suppression with wavenumber notch filtering for various acquisition geometries" by Gulunay et al. (*EAGE* 2005 *Extended Abstracts*). "3D seismic horizon-based approaches to fracture-swarm sweet spot definition in tight-gas reservoirs" by Hart et al. (*TLE*, 2002). "Fast structural interpretation with structure-oriented filtering" by Hoecker and Fehmers (*TLE*, 2002). "Automatic fault extraction using the double Hough transform" by Jacquemin and Mallet (*SEG 2005 Expanded Abstracts*). "Edge preserving filtering on 3D seismic data using complex wavelet transforms" by Jervis (*SEG 2006 Expanded Abstracts*). "Snakes: Active contour models" by Kass et al. (*International Journal of Computer Vision*, 1988). "Wavelet-based detection of singularities in acoustic impedances from surface seismic reflection data" by Li and Liner (GEOPHYSICS, 2008). "Detection of zones of abnormal strains in structures using Gaussian curvature analysis" by Lisle (AAPG *Bulletin*, 1994). "Edge-preserving smoothing and applications" by Luo et al. (*TLE*, 2002). "Robust estimates of reflector dip and azimuth" by Marfurt (GEOPHYSICS, 2006). "Narrow-band spectral analysis and thin-bed tuning" by Marfurt and Kirlin (GEOPHYSICS, 2001). "Definition of depositional geological elements in deep-water minibasins of the Gulf of Mexico using spectral decomposition in depth domain" by Montoya et al. (*SEG 2005 Expanded Abstracts*). "Interpretational applications of spectral decomposition in reservoir characterization" by Partyka et al. (*TLE*, 1999). "New azimuthal binning for improved delineation of faults and fractures" by Perez and Marfurt (submitted to GEOPHYSICS). "Automatic extraction of fault surfaces from three-dimensional seismic data" by Randen et al. (*SEG 2001 Expanded Abstracts*). "Using spectral decomposition and coherence for reservoir delineation and fluid prediction in extensively explored region" by Rauch-Davies and Graham (*SEG 2006 Expanded Abstracts*). "Spectral decomposition—transform methods and fluid and reservoir prediction case study" by Rauch-Davies and Ralston (*EAGE 2005 Extended Abstracts*, 2007). "Attribute extraction: An important application in any 3D seismic interpretation" by Rijks and Jauffred (*TLE*, 1991). "Better understanding Wyoming reservoirs through co-visualization and analysis of 3D seismic, VSP, and engineering data—Teapot Dome, Powder River Basin" by Roth et al. (2005 RMAG/DGS 3D Seismic Symposium). "Spectral decomposition of seismic data with continuous-wavelet transforms" by Sinha et al. (GEOPHYSICS, 2005). "Visualization techniques for enhancing stratigraphic inferences from 3D seismic data volumes" by Stark (*First Break*, 2006). "Teaching old attributes new tricks: Implications of 3D instantaneous phase unwrapping" by Stark (Geophysical Society of Houston, SEG Spring Symposium 2007). "Why interpret with seismic attributes? Caveats, keynotes, and a case study featuring multiple seismic attribute analysis in hydrothermal dolomite" by Strecker et al. (2005 SIPES 3D Symposium). "Complex seismic trace analysis" by Taner et al. (GEOPHYSICS, 1979). "A robust method for Q estimation" by Taner and Treitel (*SEG 2003 Expanded Abstracts*). "Inverse Q-filter for seismic resolution enhancement" by Wang (GEOPHYSICS, 2006). "Successful application of spectral decomposition technique to map deep gas reservoirs" by Wankui et al. (*SEG 2006 Expanded Abstracts*). "Interactive seismic facies classification using textural and neural networks" by West et al. (*TLE*, 2002). **TLE**

*Acknowledgments: We thank Arcis Corporation for permission to publish the data in figures 1, 2, 4, 5, 7, 8, 9, 10, and 13. Figure 18 is courtesy of Dengliang Gao of Marathon Oil and Figure 19 is courtesy of the Rocky Mountain Oilfield Technology Center.*

*Corresponding author: schopra@arcis.com*